Multipole Moment Preserving Condensation of Volumetric Acoustic Sources

P. Croaker (1), S. Marburg (2), R. Kinns (1), N. Kessissoglou (1)

(1) School of Mechanical & Manufacturing Engineering, The University of New South Wales, Sydney, NSW 2052, Australia
(2) LRT4 – Institute of Mechanics, Universität der Bundeswehr München, D-85579 Neubiberg, Germany

ABSTRACT

A meshfree multipole moment preserving condensation (M*m*MPC) method is proposed to spatially condense the volumetric quadrupole sources based on Lighthill's acoustic analogy that are extracted from computational fluid dynamics (CFD) data. The purpose of the method is to reduce both the amount of data that must be stored during the CFD analysis and the number of acoustic sources driving the subsequent acoustic propagation analysis, while preserving the accuracy of the predicted sound pressure field. The method uses a distribution of particles with quintic kernels to integrate the acoustic sources and employs a multipole expansion of the harmonic free-field Green's function to preserve the multipole moments of the underlying acoustic sources. The directivity of the sound pressure field due to the quadrupole sources are presented for the first four harmonics of the vortex shedding frequency for flow past a circular cylinder with Reynolds number, Re_D=100 and Mach number, M=0.02. Using the M*m*MPC method, the number of acoustic sources is reduced by a factor of 120 with the associated far-field sound pressure levels within 0.5 dB of the non-condensed results for all four harmonics.

INTRODUCTION

Lighthill (1952, 1954) reformulated the Navier-Stokes equation into a wave equation that represents the acoustic source generation by fluid motion and the propagation of these acoustic sources. He derived an acoustic analogy that demonstrates sound generated by a turbulent fluid flow is equivalent to the sound generated by a distribution of acoustic quadrupoles computed from the instantaneous velocity fluctuations. The acoustic sources are extracted from the transient flow field data and then a wave equation, derived from Lighthill's acoustic analogy, is solved to predict the propagation of these acoustic sources.

An important result from Lighthill's work is that the acoustic source terms can be calculated from hydrodynamic flow field variables. This has prompted the development of a wide range of hybrid methods which use CFD to calculate acoustic source terms from transient flow variables and Lighthill's acoustic analogy to predict the acoustic propagation. These hybrid methods typically make use of the Green's function solution of the wave equation to reformulate the acoustic propagation problem into a boundary integral equation (BIE). The most common approach is to employ a free-field Green's function or its spatial derivatives to predict the propagation of the acoustic sources.

If the acoustic propagation is performed in the frequency domain, the entire time history of Lighthill's stress tensor must be stored for each CFD cell. Even if the acoustic propagation is performed in the time domain, a significant portion of the time history must still be stored as this approach relies on retarded, or forward, time to propagate the individual acoustic sources to the field points. Both of these approaches have a significant data storage requirement. Additionally, the propagation of each acoustic source point to each field point must be calculated separately using the Green's function or its derivatives. For high Reynolds number flows, the CFD model will typically contain a large number of cells and hence a large amount of acoustic source data will need to be stored. This will result in a potentially huge data storage requirement and time consuming acoustic propagation analysis.

This paper presents a method to spatially condense the volumetric sources of Lighthill's acoustic analogy, significantly reducing the number of acoustic sources that are stored and the number of propagation calculations that must be performed. BIE does not have a volume mesh that can be used to integrate or interpolate the acoustic source data extracted from the CFD results. Hence, a meshfree method is proposed to spatially condense the acoustic source data. Suleau and Bouillard (2000) have applied meshfree methods to solve the Helmholtz equation on a distribution of particles or nodes. All of these methods suffer from dispersion errors. However, He et al. (2011) demonstrated that with careful selection of particle properties, the dispersion errors of these meshfree methods are considerably less than those obtained with many FEM implementations. Golberg et al. (2000) used meshfree radial basis functions, in conjunction with the dual reciprocity method, to convert the volume integral into a series of boundary integrals. The solution of these boundary integrals then provides the particular solution of the Helmholtz equation due to the volume distribution of sources. In the present method, a distribution of particles is overlaid on the CFD mesh. The resolution of these particles is coarser than the underlying CFD mesh. A particle approximation of the volume integral is then obtained in conjunction with a multipole expansion of the harmonic free-field Green's function, relative to each particle's centre, to spatially condense the acoustic source data. The net result of this approach is that only the multipole moments of the Lighthill tensor components relative to the particle centre needs to be stored. The Green's functions and their derivatives then only need be evaluated at each particle centre for each field point. The combination of a particle method approximation of the volume integral in Lighthill's acoustic analogy, coupled with the multipole expansion of the Green's function within each particle's smoothing length, results in significant savings to both the data storage requirements and the number of calculations required for the acoustic propagation analysis.

The Meshfree multipole Moment Preserving Condensation (M*m*MPC) method is used to predict the far-field sound pressure produced by the volumetric quadrupole sources arising from laminar flow past a cylinder at a Reynolds number, Re_D=100 and Mach number, M=0.02. The radiated sound pressure due to the volumetric quadrupole sources of Lighthill's acoustic analogy is predicted with and without the spatial condensation and the accuracy of the method is demonstrated. It is noted that the dominant sound produced by vortex shedding from a cylinder is of a dipolar nature and is caused by the scattering of the volu-

metric quadrupole sources by the surface of the cylinder. The present method does not consider this scattered sound field and deals only with the direct radiation of the volume quadrupoles to the far-field. Future work will extend the M*m*MPC method to include the sound field scattered from a body.

NUMERICAL METHODS

Background - Lighthill's Acoustic Analogy

Lighthill's acoustic analogy is given by (Lighthill 1952,1954):

$$\frac{\partial^2 \rho}{\partial t^2} - c_0^2 \frac{\partial^2 \rho}{\partial x_i^2} = \frac{\partial^2 T_{ij}}{\partial x_i \partial x_j} \tag{1}$$

where ρ is the fluid density and c_0 is the speed of sound in the medium at rest. T_{ij} is the Lighthill tensor and is given by:

$$T_{ij} = \rho u_i u_j + \left(p - c_0^2 \rho\right) \delta_{ij} - \tau_{ij} \tag{2}$$

where p is the pressure, u_i and u_j are the i^{th} and j^{th} components of the velocity vector respectively, δ_{ij} is the kronecker delta and τ_{ij} is the viscous stress tensor. The first term on the right hand side of equation (2) represents the contribution due to the Reynolds stresses. The second term relates to sound generation by non-isotropic processes and the third term represents the contributions due to viscous stresses. The ultimate application of this work is for low Mach number, high Reynolds number flows. For such a flow regime, it is reasonable to approximate Lighthill's tensor by:

$$T_{ij} = \rho_0 u_i u_j \tag{3}$$

where ρ_0 is the incompressible fluid density. In what follows, a harmonic time dependence of $e^{-i\omega t}$ has been assumed. An expression for calculating the acoustic pressure, p_a, at a field point, $\mathbf{x}$, due to the direct radiation of the quadruole sources in a finite volume, Ω, is given by:

$$\hat{p_a}(\mathbf{x}) = -\int_\Omega \hat{T}_{ij} \frac{\partial^2 G_k(\mathbf{x},\mathbf{y})}{\partial y_i \partial y_j} d\mathbf{y} \tag{4}$$

where G_k is the harmonic Green's function. Equation (4) is the harmonic integral formulation for Lighthill's acoustic analogy. Note that the scattering and diffraction of sound caused by a rigid body is not considered in the present work.

Multipole Moment Preserving Condensation Method

The fundamental concept of the spatial condensation method is to overlay a distribution of particles over the CFD mesh. A particle approximation of the volume integral in equation (4) is then used to calculate the contribution of the volumetric acoustic sources to the acoustic pressure. The method also makes use of a Taylor series expansion of the quadrupole kernel of the harmonic Green's function on a particle-by-particle basis. These two concepts combine to offer significant reduction in the amount of data that must be stored during the CFD simulation and the number of calculations that must be performed to evaluate the volume integral.

To formulate a particle approximation of the volume integral in equation (4), the following function is defined:

$$f(\mathbf{x},\mathbf{y}) = \hat{T}_{ij}(\mathbf{y}) \frac{\partial^2 \hat{G}_k(\mathbf{x},\mathbf{y})}{\partial y_i \partial y_j} \tag{5}$$

Using the unique properties of the Dirac Delta function given by:

$$\delta(\mathbf{y}-\mathbf{y}') = \begin{cases} \infty, & \mathbf{y}=\mathbf{y}' \\ 0, & \mathbf{y}\neq\mathbf{y}' \end{cases} \tag{6}$$

$$\int_\Omega \delta(\mathbf{y}-\mathbf{y}') = 1 \tag{7}$$

equation (5) can be expressed as:

$$f(\mathbf{x},\mathbf{y}) = \int_\Omega f(\mathbf{x},\mathbf{y}')\delta(\mathbf{y}-\mathbf{y}')d\mathbf{y}' \tag{8}$$

Equation (8) can not be approximated in a discrete sense. To overcome this, the Delta function is replaced by a kernel function, $w(\mathbf{y}-\mathbf{y}',h)$ with finite support h. A 1D piecewise quintic kernel is used as the building block for all kernels. The 1D piecewise quintic kernel is defined by:

$$w\left(y_i - y_i', h\right) = \frac{120}{h} \begin{cases} (3-q_i)^5 - 6(2-q_i)^5 + 15(1-q_i)^5 & 0 \le q_i < 1 \\ (3-q_i)^5 - 6(2-q_i)^5 & 1 \le q_i < 2 \\ (3-q_i)^5 & 2 \le q_i \le 3 \\ 0 & q_i > 3 \end{cases} \tag{9}$$

where y_i and y_i' are the i^{th} components of the $\mathbf{y}$ and $\mathbf{y}'$ position vectors respectively and $q_i = \frac{|y_i - y_i'|}{h}$. Kernel functions for higher dimensions are constructed using tensor products of this 1D piecewise quintic kernel as follows:

$$w\left(\mathbf{y}-\mathbf{y}', h\right) = \prod_{i=1}^{R} w\left(y_i - y_i'\right) \tag{10}$$

where R is the dimension of the problem. The kernel approximation of $f(\mathbf{x},\mathbf{y})$ is then expressed as:

$$\langle f(\mathbf{x},\mathbf{y})\rangle = \int_\Omega f(\mathbf{x},\mathbf{y}')w(\mathbf{y}-\mathbf{y}',h)d\mathbf{y}' \tag{11}$$

where the smoothing length, h, is the size of the compact support of the smoothing function. Using the kernel approximation given by equation (11), equation (5) can be expressed as:

$$\langle f(\mathbf{x},\mathbf{y})\rangle = \int_\Omega \hat{T}_{ij}(\mathbf{y}') \frac{\partial^2 G_k(\mathbf{x},\mathbf{y}')}{\partial y_i \partial y_j} w(\mathbf{y}-\mathbf{y}',h)d\mathbf{y}' \tag{12}$$

In what follows, it is assumed that hydrodynamic flow variables and hence the Lighthill stress tensor components, $\hat{T_{ij}}(\mathbf{y}')$, are available on a CFD mesh. It is also assumed that the CFD cell centre coordinates, $\mathbf{y}_n$, and cell volumes, $\triangle V_n$, are known. To make use of the kernel approximation of equation (12), a distribution of particles is overlaid over the CFD mesh. Figure 1 shows an example of a particle distribution overlaid on a CFD mesh. In Figure 1, $\mathbf{x}$ is the field point, $\mathbf{y}_p$ and $\mathbf{y}_n$ are the coordinates of the centre of the pth particle and nth CFD cell respectively, r is the distance separating $\mathbf{x}$ and $\mathbf{y}_p$, h is the smoothing length of the particle and is typically defined as a ratio of particle spacing, d.

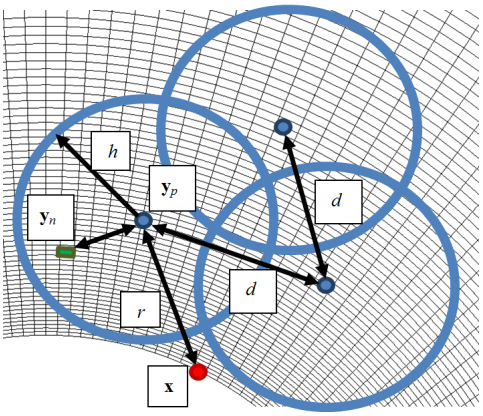

Figure 1: Schematic diagram of spatial condensation method

For a particular particle, p, the discrete kernel approximation of the function $f(\mathbf{x},\mathbf{y})$ based on the underlying CFD cell variables is given by:

$$\langle f(\mathbf{x},\mathbf{y}_p)\rangle = \sum_{n=1}^{N} \hat{T}_{ij}(\mathbf{y}_n) \frac{\partial^2 G_k(\mathbf{x},\mathbf{y}_n)}{\partial y_i \partial y_j} w(\mathbf{y}_p - \mathbf{y}_n, h) \triangle V_n \tag{13}$$

where N is the total number of nodes within the particle's smoothing length. To simplify the expressions, the following abbreviations are used:

$$\begin{aligned} T_{ijn} &= T_{ij}(\mathbf{y}_n) \\ w_{p,n} &= w(\mathbf{y}_p - \mathbf{y}_n, h) \end{aligned}$$

In its current form, the discrete kernel approximation given in equation (13) requires the evaluation of the second derivative of the harmonic Green's function for all CFD cells for each field point, $\mathbf{x}$. This provides no savings in computational expense over directly evaluating the volume integral of equation (4). A more efficient approach is achieved by performing a Taylor series expansion of the second derivative of the harmonic Green's function for all CFD cells within the compact support of the particle's kernel function, around the centre of the particle. Thus, the discrete approximation of the function is expressed as:

$$\begin{aligned} \left\langle f(\mathbf{x},\mathbf{y}_p)\right\rangle &= \sum_{n=1}^{N} \hat{T_{ijn}} \left(\sum_{m_1=0}^{\infty} \cdots \sum_{m_R=0}^{\infty} \frac{(y_{1p}-y_{1n})^{m_1} \cdots (y_{Rp}-y_{Rn})^{m_R}}{m_1! \cdots m_R!} \right. \\ &\left. \times \frac{\partial^{2+m_1+\cdots+m_R} G_k(\mathbf{x},\mathbf{y}_p)}{\partial y_i \partial y_j \partial y_1^{m_1} \cdots \partial y_R^{m_R}} \right) w_{p,n} \triangle V_n \end{aligned} \quad (14)$$

where m_1 to m_R represents the order of the expansion in the 1 through R coordinate directions, respectively. y_{1p} to y_{Rp} represents the 1st to Rth component of the position vector $\mathbf{y}_p$ and similarly, y_{1n} to y_{Rn} are the 1st to R^{th} components of the position vector $\mathbf{y}_n$. Reorganising equation (14) produces the following:

$$\begin{aligned} \left\langle f(\mathbf{x},\mathbf{y}_p)\right\rangle &= \left(\sum_{n=1}^{N} \hat{T_{ijn}} w_{p,n} \triangle V_n \right) \frac{\partial^2 G_k(\mathbf{x},\mathbf{y}_p)}{\partial y_i \partial y_j} + \\ &\sum_{k=1}^{R} \left(\sum_{n=1}^{N} (y_{kp}-y_{kn}) \hat{T_{ijn}} w_{p,n} \triangle V_n \right) \frac{\partial^3 G_k(\mathbf{x},\mathbf{y}_p)}{\partial y_i \partial y_j \partial y_k} + \\ &\sum_{k=1}^{R} \sum_{l=1}^{R} \frac{1}{2} \left(\sum_{n=1}^{N} (y_{kp}-y_{kn})(y_{lp}-y_{ln}) \hat{T_{ijn}} w_{p,n} \triangle V_n \right) \\ &\times \frac{\partial^4 G_k(\mathbf{x},\mathbf{y}_p)}{\partial y_i \partial y_j \partial y_k \partial y_l} + \cdots \end{aligned} \quad (15)$$

where y_{kp} and y_{kn} represent the k^{th} component of the position vectors $\mathbf{y}_p$ and $\mathbf{y}_n$, respectively. Similarly, y_{lp} and y_{ln} represent the l^{th} component of the position vectors $\mathbf{y}_p$ and $\mathbf{y}_n$, respectively. The discrete approximation given by equation (15) only requires evaluation of the spatial derivatives of the Green's function at the centre of the kernel. However the trade-off is that higher order spatial derivatives of the Green's function are required. The next step is to sum the contributions to the acoustic pressure from the total number of particles, P, that are overlaid on the CFD mesh for a particular field point $\mathbf{x}$ as follows:

$$\begin{aligned} p(\mathbf{x}) &= \sum_{p=1}^{P} \left\langle f(\mathbf{x},\mathbf{y}_p)\right\rangle \\ &= \sum_{p=1}^{P} \left(\sum_{n=1}^{N} \hat{T_{ijn}} w_{p,n} \triangle V_n \right) \frac{\partial^2 G_k(\mathbf{x},\mathbf{y}_p)}{\partial y_i \partial y_j} + \\ &\sum_{p=1}^{P} \sum_{k=1}^{D} \left(\sum_{n=1}^{N} (y_{kp}-y_{kn}) \hat{T_{ijn}} w_{p,n} \triangle V_n \right) \frac{\partial^3 G_k(\mathbf{x},\mathbf{y}_p)}{\partial y_i \partial y_j \partial y_k} + \\ &\sum_{p=1}^{P} \sum_{k=1}^{D} \sum_{l=1}^{D} \frac{1}{2} \left(\sum_{n=1}^{N} (y_{kp}-y_{kn})(y_{lp}-y_{ln}) \hat{T_{ijn}} w_{p,n} \triangle V_n \right) \\ &\times \frac{\partial^4 G_k(\mathbf{x},\mathbf{y}_p)}{\partial y_i \partial y_j \partial y_k \partial y_l} + \ldots \end{aligned} \quad (16)$$

With this approach it is common for a CFD cell to lie within the smoothing length of multiple particles, as seen in Figure 1. The sum of the particle weightings applied to the nth CFD cell is given by:

$$W_n = \sum_{p=1}^{P} w_{p,n}$$

For the applied method to be globally conservative, $W_n = 1$ for all CFD cells. To ensure this condition, a scaling factor of $C_n = \frac{1}{W_n}$ is introduced for each CFD cell. Inserting the scaling factor into equation (16) gives:

$$\begin{aligned} p(\mathbf{x}) &= \sum_{p=1}^{P} \left(\sum_{n=1}^{N} \hat{T_{ijn}} C_n w_{p,n} \triangle V_n \right) \frac{\partial^2 G_k(\mathbf{x},\mathbf{y}_p)}{\partial y_i \partial y_j} + \\ &\sum_{p=1}^{P} \sum_{k=1}^{D} \left(\sum_{n=1}^{N} (y_{kp}-y_{kn}) \hat{T_{ijn}} C_n w_{p,n} \triangle V_n \right) \frac{\partial^3 G_k(\mathbf{x},\mathbf{y}_p)}{\partial y_i \partial y_j \partial y_k} + \\ &\sum_{p=1}^{P} \sum_{k=1}^{D} \sum_{l=1}^{D} \frac{1}{2} \left(\sum_{n=1}^{N} (y_{kp}-y_{kn})(y_{lp}-y_{ln}) \hat{T_{ijn}} C_n w_{p,n} \triangle V_n \right) \\ &\times \frac{\partial^4 G_k(\mathbf{x},\mathbf{y}_p)}{\partial y_i \partial y_j \partial y_k \partial y_l} + \ldots \end{aligned} \quad (17)$$

The first term on the right hand side of equation (17) represents the 0th order, or monopole moment, of the Taylor series expansion. The second term represents the 1st order, or dipole moment, and the third term represents the 2nd order, or quadrupole moment, of the Taylor series expansion. The above method is termed a 'meshfree multipole moment preserving condensation' method and is given the abreviation MmMPC, where m denotes the order of the multipole moments that are preserved. Also, m corresponds to the order of terms retained from the Taylor series expansion. For example, if only the monopole moments of the underyling acoustic sources are retained in the particle approximation, the method is given the abbreviation M0MPC. If monopole, dipole and quadrupole moments of the underlying acoustic sources are used, the method is termed M2MPC.

Equation (17) requires the summation of the Fourier transform of the components of Lighthill's tensor at each CFD cell. To compute these Fourier transforms, the time histories of Lighthill's tensor at each CFD cell must be known. In its current form, equation (17) does not reduce the amount of data that must be stored from the CFD simulation. This can be remedied by exploiting the linearity of Fourier transformations, namely:

$$\widehat{f+g} = \hat{f} + \hat{g}$$

This allows the summations in equation (17) to be performed in the time domain. Hence the summations can be performed in the CFD simulation as the analysis proceeds and only the resulting summations need be stored on a particle-by-particle basis. For each particle, the amount of data that must be saved depends on the order of the retained terms. In a three-dimensional analysis, there are one, four and ten terms required per particle for each component of Lighthill's stress tensor for the M0MPC, M1MPC and M2MPC spatial condensations, respectively. For a two-dimensional analysis this becomes one, three and six terms for each component. In order to reduce the data storage requirements and computational burden of the acoustic propagation analysis, the total number of particles must be significantly less than the total number of CFD cells.

Truncation of the Flow Domain

Impact on Hydrodynamic Analysis

If vortical structures reach the outlet boundary of the CFD domain, pressure disturbances can occur that contaminate the flow field and hence the acoustic source data. There are a number of techniques to reduce these pressure disturbances. Boundary conditions that attempt to emulate the Sommerfeld radiation condition can be applied to the outlet boundaries. These boundary conditions are designed to allow the vortical structures to pass through the outlet with very little reflection and hence minimal pressure disturbance. Examples of such 'non-reflecting' boundary conditions include the convective boundary condition derived by Orlanski (1976) and the Navier-Stokes characteristic boundary condition of Poinsot and Lele (1992). Another

approach, proposed by Israeli and Orszag (1981), is to apply additional damping to the fluctuating flow field in a 'sponge layer' upstream of the boundary so that all vortical structures have been dissipated before they reach the outlet. In this work, a sponge layer was created immediately upstream of the boundary, with its viscosity artificially increased by a factor of 35.

Impact on Acoustic Analysis

Derivation of equation (4) relies on Gauss' divergence theorem and the fact that the Lighthill stress tensor equals zero at the infinite bounds of the domain. The implicit assumption in these derivations is that the Lighthill tensor also vanishes on the boundary of the CFD model. This assumption requires that the flow domain is large enough that there are no velocity fluctuations at the boundary. Perez et al. (2007) demonstrate that when T_{ij} is non zero on the boundary of the flow domain, the accuracy of the acoustic propagation analysis can suffer severely. This requirement on flow domain size is not practical for most flows of interest and hence steps must be taken to address the issue. Several methods have been used previously. Caro et al. (2009) used a spatial window function to artificially force the Lighthill tensor to zero at the boundary of the computational domain. Perez et al. (2007) accounted for non-zero Lighthill stress tensor boundary values in the derivation of the acoustic propagation equations. Wang et al. (1996) approximated the values of the Lighthill stress tensor outside the flow domain from the computed values inside. Martínez-Lera and Schram (2008) provide a good review of available techniques. They investigated the effect that different source truncation treatments have on the predicted far-field sound pressure field.

In the present work, a simple spatial window function has been applied to the Lighthill stress tensor. This window function has the following shape:

$$\phi(r) = \begin{cases} 1 & 0 \le r \le 10 \\ 0.5\left(1+\cos\left(\frac{\pi(r-10)}{20}\right)\right) & 10 < r \le 30 \\ 0 & r > 30 \end{cases} \quad (18)$$

The sponge layer described in the previous section will reduce the velocity fluctuations and thereby the Lighthill stress tensor at the boundary. However, there is no way to guarantee beforehand that the value of the Lighthill stress tensor will vanish on the boundary, hence the spatial window function is also applied.

Transient Laminar CFD Simulation

To demonstrate the M*m*MPC method, laminar vortex shedding from a cylinder of diameter D is simulated at $Re_D = 100$ and $M = 0.02$. A two-dimensional circular domain around the cylinder has been modelled and analysed using ESI Group's CFD-ACE+ software package. The velocity-pressure form of the Navier-Stokes equations are solved by CFD-ACE+ and in this instance, a direct numerical simulation (DNS) of the flow field has been performed. The Navier-Stokes equations are given by:

$$\begin{aligned} \frac{\partial(\rho u_x)}{\partial t} + \nabla\cdot(\rho \mathbf{u} u_x) &= -\frac{\partial p}{\partial x} + \nabla\cdot(\mu \nabla u_x) + S_{Mx} \\ \frac{\partial(\rho u_y)}{\partial t} + \nabla\cdot(\rho \mathbf{u} u_y) &= -\frac{\partial p}{\partial y} + \nabla\cdot(\mu \nabla u_y) + S_{My} \\ \frac{\partial(\rho u_z)}{\partial t} + \nabla\cdot(\rho \mathbf{u} u_z) &= -\frac{\partial p}{\partial z} + \nabla\cdot(\mu \nabla u_z) + S_{Mz} \end{aligned} \quad (19)$$

where $\mathbf{u} = (u_x, u_y, u_z)$ is the velocity vector and S_{Mx}, S_{My} and S_{Mz} are momentum source terms in the x, y and z directions, respectively. CFD-ACE+ uses an iterative, segregated solution method with the pressure-velocity coupling handled using the SIMPLEC algorithm.

The model used for the CFD simulation is shown in Figure 2, with the mesh topology in the vicinity of the cylinder inset.

The interior of the computational domain extends radially for 25D. A sponge layer extends radially for an additional 20D. The interior domain contains 71,760 quadrilateral cells, with a cell spacing adjacent to the cylinder of 0.005D. The cell distribution is biased so that the wake region contains a high cell density to resolve the vortices shed from the cylinder. The sponge layer contains an additional 6,960 quadrilateral cells. The cell size on either side of the interface between the interior domain and sponge layer is uniform, with the cells in the sponge layer then growing rapidly in the radial direction.

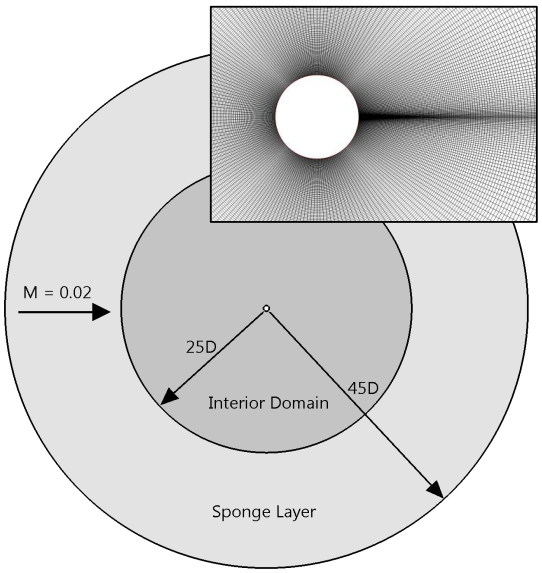

Figure 2: Domain shape and size for CFD analysis

The viscosity in the sponge layer has been artificially increased by a factor of 35 to damp out the fluctuations in the velocity field in an attempt to force the acoustic source terms to zero at the boundary. A steady state simulation was performed with the converged solution used as the initial condition of the transient simulation. The simulations were second order accurate in time and space, with a central difference scheme used for the spatial discretisation and a Crank-Nicholson scheme used for the temporal discretisation. The transient simulation was executed with a time step size of 2.99E-5s and was allowed to progress until the flow field achieved periodicity. Recording of the acoustic source data commenced after this periodicity had been attained and data from eight vortex shedding periods was obtained.

Far-field Sound Pressure Level

The field points were placed on a circle of radius 6000D centred on the cylinder in 2.5° increments with 0° aligned with the direction of fluid flow. The method presented here has been developed for three-dimensional applications and hence the acoustic propagation was also carried out in three dimensions. As the two-dimensional hydrodynamic simulation assumes that the cylinder is infinitely long, to approximate the acoustic propagation in three dimensions, the cylinder was assumed to have a finite length of 42,600D. The contribution to the sound pressure at a field point, $\mathbf{x}$, due to a source point located on the cylinder end plane has a magnitude of approximately 0.02 relative to the same source located at the cylinder mid plane. This length was divided into 7,100 equal intervals of 6D, ensuring that at least 12 adjacent sources reach the field point within the same wavelength to prevent aliasing of the propagated sound field. Acoustic sources were extracted from the two-dimensional hydrodynamic data. Assuming an out-of-plane cell depth of 6D, 7,100 identical copies of these acoustic sources were then created. For the particle approximation a similar approach was adopted, that is, a particle distribution was overlaid on the two-

dimensional mesh and the acoustic sources were calculated for each particle. 7,100 identical copies of these acoustic sources were then created in the out-of-plane direction. Hence, even though the resulting acoustic propagation analysis is conducted in three dimensions, the spatial condensation is only applied in two dimensions. In the discussion on the accuracy of the MmMPC method, the number of particles created in two dimensions are used as the reference.

RESULTS AND DISCUSSION

Hydrodynamic Analysis

Figure 3 shows a snap shot of the vorticity in the flow field, with the black arcs representing the boundary of the sponge layer. Figure 3 shows that the sponge layer is effective in damping out the vorticity before reaching the downstream boundary.

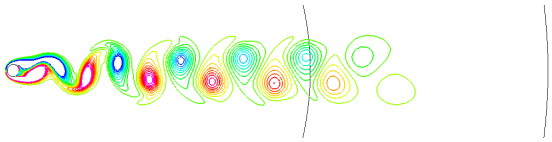

Figure 3: Vorticies in wake of cylinder. The contours are of vorticity, ω, with levels from $\omega_{min} = -100\,s^{-1}$ to $\omega_{max} = 100\,s^{-1}$ with an increment of $10\,s^{-1}$

Figure 4 shows the frequency spectra of the fluctuating lift and drag forces exerted on the cylinder. The fundamental vortex shedding frequency occurs at 16.5 Hz. This figure also illustrates that peaks of the fluctuating lift force occur at odd harmonics of the vortex shedding frequency and peaks of the drag force occur at even harmonics. The mean drag coefficient calculated from the transient CFD simulation is $C_D = 1.32$ which compares well with the experimental value of 1.24 to 1.26 obtained by Tritton (1959). The Strouhal number predicted from the present analysis is $St = 0.165$ and is in very close agreement with the experimental value of 0.164 reported by Fey et al. (1998).

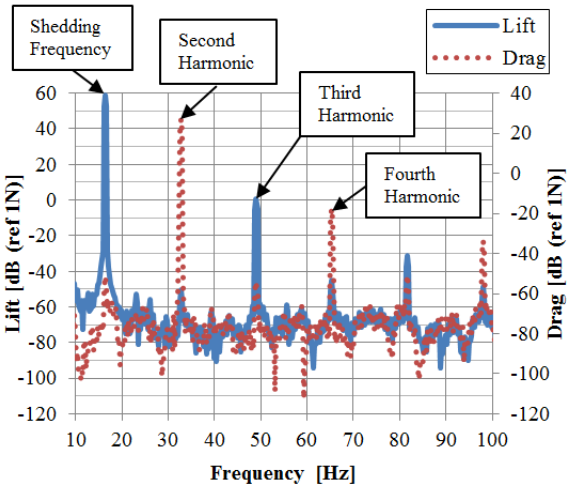

Figure 4: Frequency spectra of the lift and drag forces

Based on published simulation data for laminar shedding from circular cylinders in cross flow, Norberg (2001) developed an empirical relationship to approximate the RMS of the fluctuating lift force based on the Reynolds number. The RMS of the fluctuating lift force predicted from the present analysis is 0.218, which compares well with the approximate value of 0.227 obtained using the empirical relationship of Norberg (2001).

Acoustic Source Extraction

Figures 5, 6 and 7 show the magnitude and phase of the T_{11}, T_{12} and T_{22} components of Lighthill's tensor, respectively, for the CFD simulation including the sponge layer. These acoustic sources are used to compute the far-field sound pressure and are also used as the underlying data for the MmMPC.

Far-field Directivity of Non-Condensed Sources

The contribution to the far-field sound pressure from the non-condensed volumetric acoustic sources was calculated directly using equation (4). Figure 8 shows the far-field sound pressure for the first four harmonics of the vortex shedding frequency. These results are used as a reference to determine the accuracy of the MmMPC method.

Accuracy of the MmMPC Method

Figure 9 shows the directivity of the sound pressure predicted by the monopole condensation method (M0MPC) for the first four harmonics of the vortex shedding frequency and for four particle distributions, $P = 633$, 1737, 6799 and 27417. A particle smoothing length of $h = 1.2d$ was used. There is no appreciable difference between the non-condensed and spatially condensed results for the first three harmonics of the vortex shedding frequency. For the fourth harmonic there is an obvious discrepancy between the non-condensed results and the spatially condensed results for coarser distributions of particles. However as the particle distribution increases, the error between the non-condensed and spatially condensed results becomes negligible.

Figure 10 (a) and (b) shows the impact of higher order spatial condensation on the accuracy of the predicted sound pressure directivity at the fourth harmonic, for $P = 663$ and $P = 1737$, respectively. A particle smoothing length of $h = 1.2d$ was used. For both cases, the accuracy is considerably improved by increasing the order of the spatial condensation. However, the number of acoustic propagation calculations per particle increases with the order of spatial condensation. For the two-dimensional condensation considered here, there is one propagation calculation per particle for M0MPC, three for M1MPC and six for M2MPC per component of Lighthill's tensor.

The accuracy for the M0MPC case, with $P = 663$ and hence 663 calculations per field point per component of Lighthill's tensor, is within approximately 6%, or 0.5 dB, for the 4th harmonic frequency, and has significantly greater accuracy at lower frequencies. This represents a reduction by a factor of approximately 120 on the amount of data that must be stored during the CFD simulation and on the number of acoustic propagation calculations that must be performed. For the M2MPC case, with $P = 663$ and hence 3978 calculations per field point per component of Lighthill's tensor, the accuracy is within approximately 0.4%, or 0.04 dB, with a reduction by a factor of 20 on the data storage and acoustic propagation calculations.

CONCLUSIONS

A particle method has been developed to approximate the volume integral of Lighthill's acoustic analogy. The MmMPC method has been applied to predict the flow induced noise directly produced by the volumetric acoustic sources. The method extracts the acoustic sources along with their multipole moments about the particle centres from incompressible CFD data. This results in a significant saving in the amount of data that must be stored during the CFD analysis as the particle distribution can be much coarser than the underlying CFD mesh. The method also makes use of a Taylor series expansion of the Green's function about the particle centres and then predicts

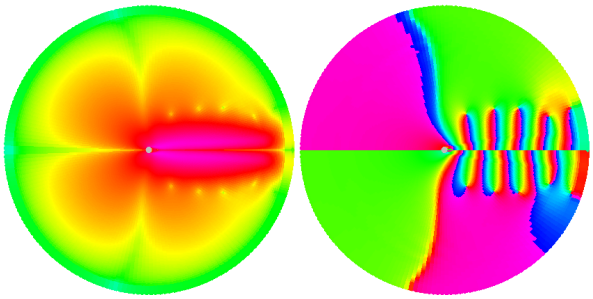

(a) Vortex shedding frequency

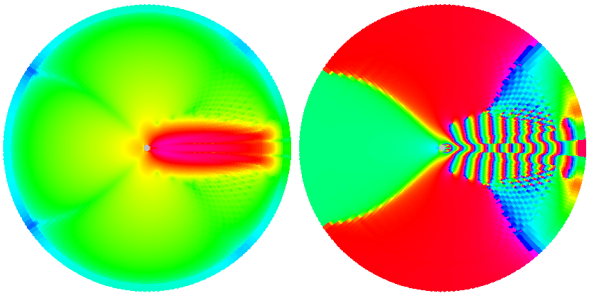

(b) 2nd harmonic frequency

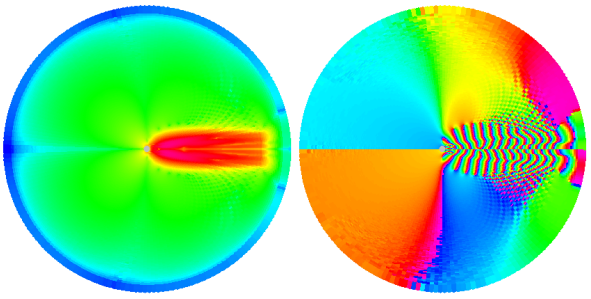

(c) 3rd harmonic frequency

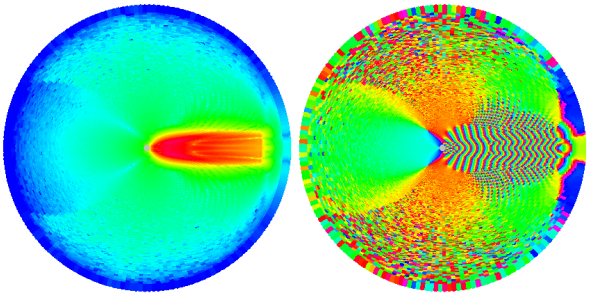

(d) 4th harmonic frequency

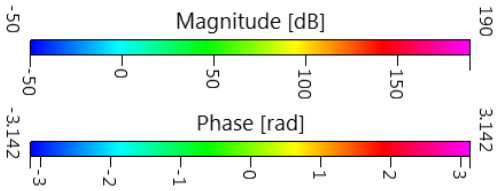

Figure 5: Magnitude (left) and phase (right) of the T_{11} component of Lighthill's quadrupole source term.

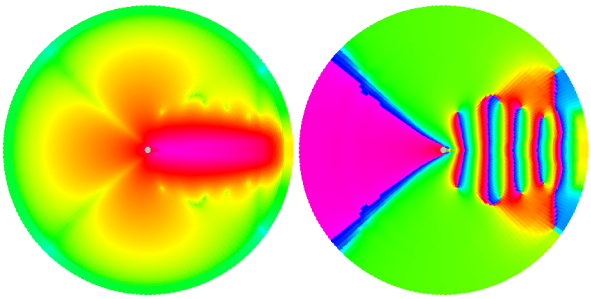

(a) Vortex shedding frequency

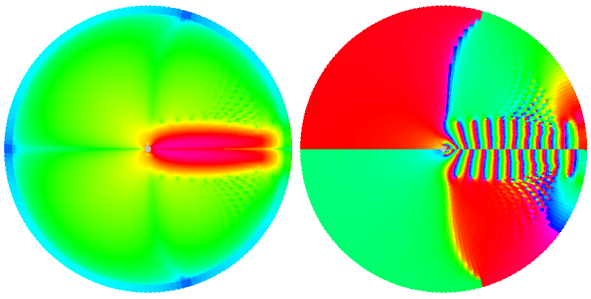

(b) 2nd harmonic frequency

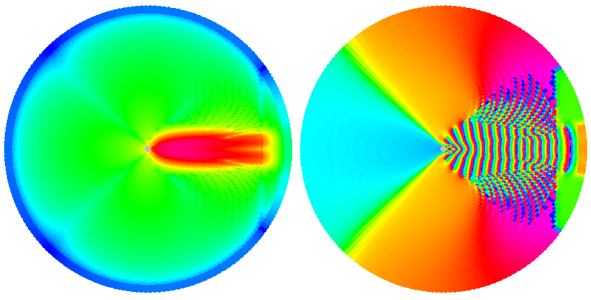

(c) 3rd harmonic frequency

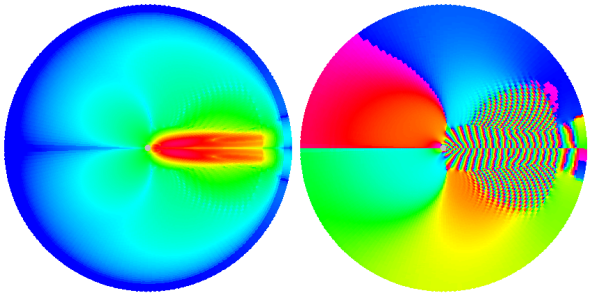

(d) 4th harmonic frequency

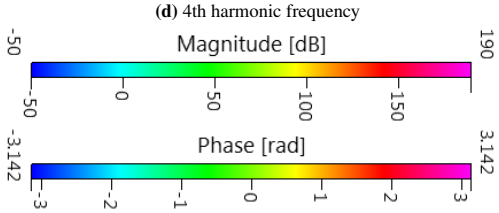

Figure 6: Magnitude (left) and phase (right) of the T_{12} component of Lighthill's quadrupole source term.

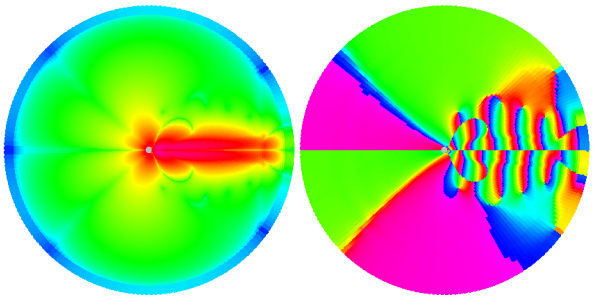

(a) Vortex shedding frequency

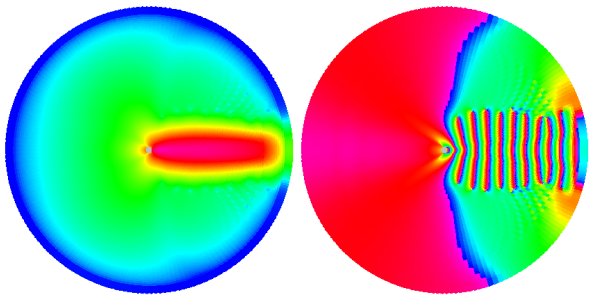

(b) 2nd harmonic frequency

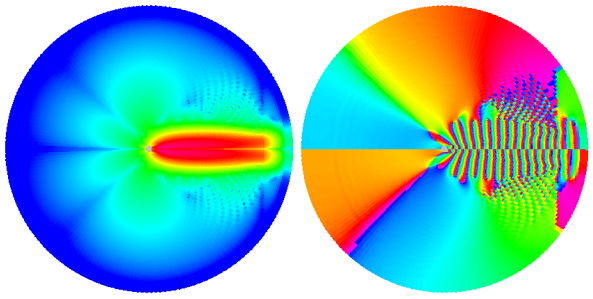

(c) 3rd harmonic frequency

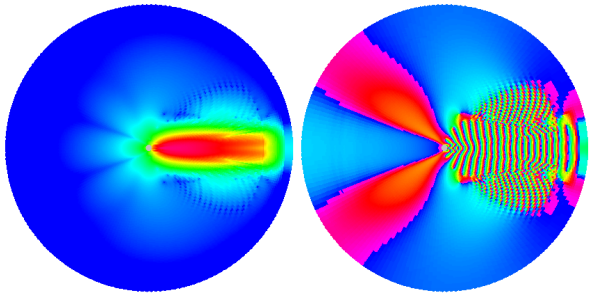

(d) 4th harmonic frequency

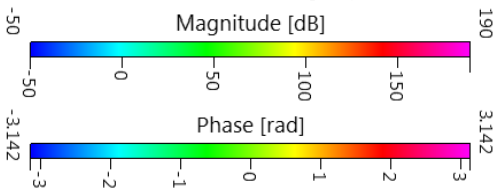

Figure 7: Magnitude (left) and phase (right) of the T_{22} component of Lighthill's quadrupole source term.

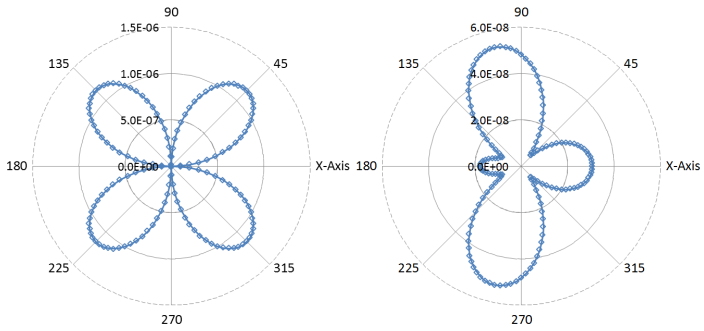

(a) Vortex shedding frequency **(b)** 2nd harmonic frequency

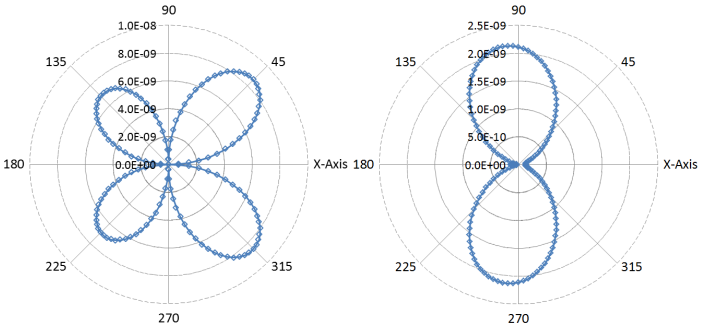

(c) 3rd harmonic frequency **(d)** 4th harmonic frequency

Figure 8: Directivity of the quadrupole pressure amplitude, $\left|\frac{\hat{p_a}}{\rho_0 U_\infty^2}\right|$, calculated from the non-condensed volumetric sources at $r = 6000D$, for the first four harmonics of the vortex shedding freqency

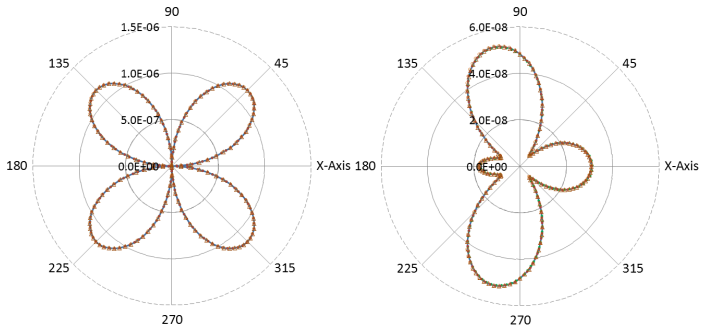

(a) Vortex shedding frequency **(b)** 2nd harmonic frequency

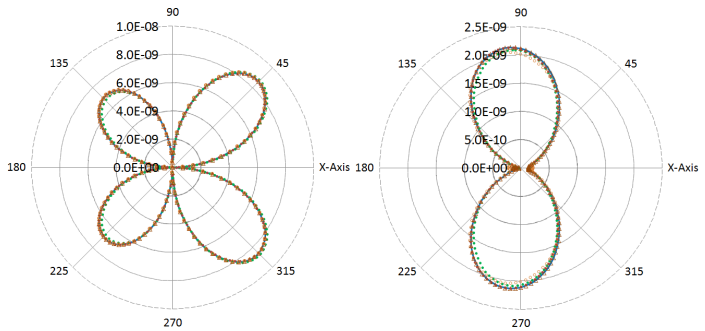

(c) 3rd harmonic frequency **(d)** 4th harmonic frequency

Figure 9: Directivity of the quadrupole pressure amplitude, $\left|\frac{\hat{p_a}}{\rho_0 U_\infty^2}\right|$, calculated from M0MPC condensation of volumetric sources relative to non-condensed sources, at $r = 6000D$, for the first four harmonics of the vortex shedding

the far field acoustic pressure by solving the harmonic wave equation using a Green's function solution. This results in a significant reduction in the number of calculations to perform the acoustic propagation analysis. The method was applied to predict the direct sound field radiated by the volume quadrupole sources in low Reynolds number flow past a circular cylinder. Using the M*m*MPC method, the amount of data stored during the CFD simulation and the number of acoustic propagation calculations were reduced by a factor of approximately 120, with the resulting sound pressure level within 0.5 dB of the non-condensed solution. In this paper it has been shown that the M*m*MPC method is capable of accurately capturing the magnitude and relative phase of the underlying volume quadrupole acoustic sources obtained from a CFD analysis.

ACKNOWLEDGEMENTS

Funding for this work has been provided by the Maritime Platforms Division of the Defence Science and Technology Organisation. Also, financial assistance from the Australian Acoustical Society (NSW Division) for an AAS NSW Travel Award to participate at the Acoustics 2011 conference is gratefully acknowledged.

REFERENCES

Caro, S, Detandt, Y, Manera, J, Toppinga, R and Mendonc a, F (2009), "Validation of a new hybrid CAA strategy and application to the noise generated by a flap in a simplified HVAC duct", *AIAA Paper 09-3352, 15th AIAA/CEAS Aeroacoustics Conference, 11-13 May 2009, Miami, Florida, USA.*

Fey, U, König, M and Eckelmann, H (1998), "A new Strouhal–Reynolds-number relationship for the circular cylinder in the range 47 < Re < 2 x 10^5", *Physics of Fluids* 10.7, pp. 1547–1549.

Golberg, MA, Chen, CS and Ganesh, M (2000), "Particular solutions of 3D Helmholtz-type equations using compactly support radial basis functions", *Engineering Analysis with Boundary Elements* 24, pp. 539–547.

He, Z, Li, P, Li, Z and Liu, G (2011), "Dispersion and pollution of the improved meshless weighted least-squares (IMWLS) solution for the Helmholtz equation", *Engineering Analysis with Boundary Elements* 35, pp. 791–801.

Israeli, M and Orszag, SA (1981), "Approximation of radiation boundary conditions", *Journal of Computational Physics* 41, pp. 115–135.

Lighthill, M (1952), "On sound generated aerodynamically, I. General theory", *Proceedings of the Royal Society A* 211, pp. 564–587.

Lighthill, M (1954), "On sound generated aerodynamically, II. Turbulence as a source of sound", *Proceedings of the Royal Society A* 222, pp. 1–32.

Martínez-Lera, P and Schram, C (2008), "Correction techniques for the truncation of the source field in acoustic analogies", *Journal of Acoustical Society of America* 124, pp. 3421–3429.

Norberg, C (2001), "Flow around a circular cylinder: Aspects of fluctuating lift", *Journal of Fluids and Structures* 15, pp. 459–469.

Orlanski, I (1976), "A simple boundary condition for unbounded hyperbolic flows", *Journal of Computational Physics* 21.3, pp. 251–269.

Perez, G, Prieur, J, Rahier, G and Vuillot, F (2007), "Theoretical and numerical discussion on volume integral methods for jet noise prediction", *AIAA paper 2007-3593, 13th AIAA/CEAS Aeroacoustics Conference, Roma, Italy, 21-23 May 2007.*

Poinsot, TJ and Lele, SK (1992), "Boundary conditions for direct simulations of compressible viscous flows", *Journal of Computational Physics* 101, pp. 104–129.

Suleau, S and Bouillard, P (2000), "One-dimensional dispersion analysis for the element-free Galerkin method for the Helmholtz equation", *International Journal for Numerical Methods in Engineering* 47, pp. 1169–1188.

Tritton, DJ (1959), "Experiments on the flow past a circular cylinder at low Reynolds numbers", *Journal of Fluid Mechanics* 6.04, pp. 547–567.

Wang, M, Lele, SK and Moin, P (1996), "Computation of quadrupole noise using acoustic analogy", *AIAA Journal* 34, pp. 2241–2254.

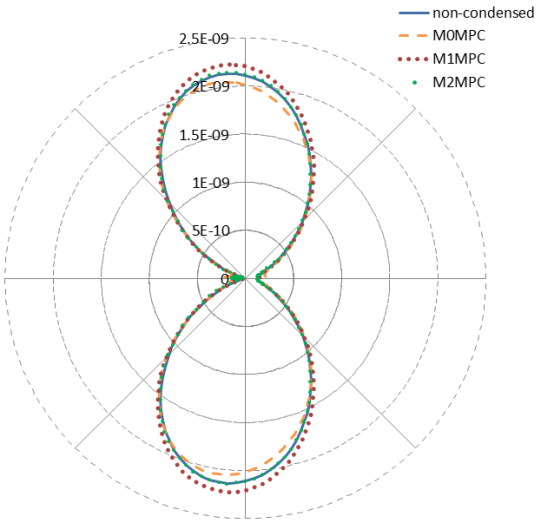

(a) $P = 663$

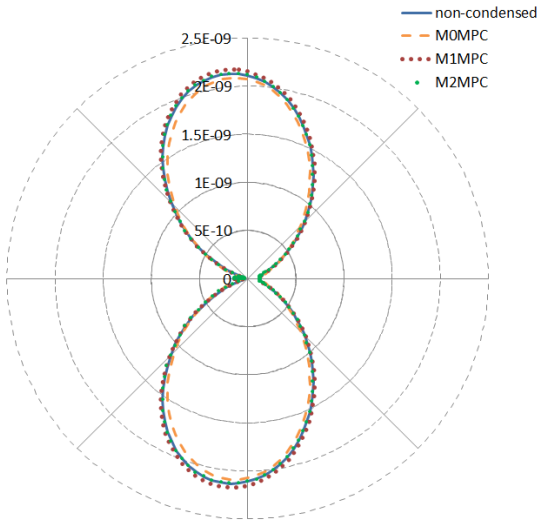

(b) $P = 1737$

Figure 10: Directivity of the quadrupole pressure amplitude, $\left|\frac{\hat{p}_a}{\rho_0 U_\infty^2}\right|$, for the fourth harmonic only, calculated from M0MPC, M1MPC and M2MPC condensation of volumetric sources relative to non-condensed sources, at $r = 6000D$